Remote Sensing of Environment 117 (2012) 19–33

Contents lists available at SciVerse ScienceDirect

Remote Sensing of Environment

journal homepage: www.elsevier.com/locate/rse

Experimental characterization and modelling of the nighttime directional anisotropy of thermal infrared measurements over an urban area: Case study of Toulouse (France)

J.-P. Lagouarde [a,*], A. Hénon [b], M. Irvine [a], J. Voogt [c], G. Pigeon [d], P. Moreau [a], V. Masson [d], P. Mestayer [b]

[a] INRA, UR1263 EPHYSE, F-33140 Villenave d'Ornon, France
[b] LMF, UMR CNRS 6598 and IRSTV, FR CNRS 2488, Ecole Centrale de Nantes, B.P. 92101, F-44321 Nantes, France
[c] Department of Geography, University of Western Ontario, London ON, Canada N6A 5C2
[d] Météo France/CNRS CNRM-GAME, 42 av Coriolis, F-31057 Toulouse, France

ARTICLE INFO

Article history:
Received 27 January 2011
Received in revised form 30 May 2011
Accepted 3 June 2011
Available online 28 September 2011

Keywords:
Anisotropy
TIR
Urban
Nighttime

ABSTRACT

The measurements of surface temperature are prone to important directional anisotropy in relation to the structure of the urban canopy and the radiative and energy exchanges inside it. Following the work of Lagouarde et al. 2010 that describes the daytime conditions, this paper focuses on the experimental analysis and modelling of the nighttime directional anisotropy. An extensive data set of airborne thermal infrared (TIR) measurements was collected over the city of Toulouse, France in the framework of the CAPITOUL project (Masson et al., 2008). The TIR measurements use a pair of thermal cameras equipped with wide angle lenses installed aboard a small aircraft. Three flights were made between 21:45 and 23:15 UTC, one in autumn and 2 in winter during 2004 and 2005 intensive operation periods (IOPs). The experimental results show that (i) the nighttime TIR directional anisotropy remains lower than 1°C for zenithal view angles up to 50°, and (ii) the nighttime anisotropy is insensitive to the azimuthal viewing direction. A modelling approach that combines a simplified 3D representation of the urban canopy with 2 energy transfer models, TEB and SOLENE, is then proposed. It confirms the experimental results quite well. Possible uncertainties on the geometry of the canopy and on most important thermo-radiative surface parameters are shown to have only little impact on the modelled TIR directional anisotropy. The time evolution of TIR anisotropy throughout night is simulated: for the fall and winter conditions studied the effects of thermal inertia completely vanish about 3 to 4 h after sunset, and the anisotropy never exceeds 2°C up to 60° zenithal view angles.

1. Introduction

The surface temperature is a key signature in the assessment of the surface energy budgets. This makes thermal infrared (TIR) remote sensing an important tool for monitoring surface processes occurring in urban areas and their practical applications (Voogt and Oke, 2003). Applications include monitoring the surface urban heat islands (SUHIs, tightly related to the air temperature UHIs), building related alert systems and improving aspects of urban planning in which the surface temperature plays a significant role. These applications are particularly important in the context of larger scale climate change that will increase the frequency and intensity of heat waves combined with increased anthropogenic fluxes derived from industrial activity, air conditioning or heating of buildings, and other urban activities such as transportation. Remotely sensed surface temperatures are also important for assessing evapotranspiration and for monitoring surface moisture and the water status of vegetation in urban areas. Improved monitoring of the surface temperature of vegetation can lead to a better assessment of the water budgets of urban watersheds (Carlson and Arthur, 2000). Vegetation is strongly related to the welfare and health of inhabitants (humidification of air, shading effects and reduction of temperatures). Evaluation of the surface temperature is also an important element for the validation of urban atmospheric flow models used for forecasting the extent of pollution plumes and improving information systems on diffusion of pollutants and air quality.

These applications require accurate measurement of the urban surface temperature. Atmospheric absorption and emission between the sensor and the surface, temperature-emissivity separation, and directional anisotropy effects all can represent an important source of error that needs specific correction. Directional anisotropy is defined here as the variation with viewing angle of the observed surface temperature Ts. It can be expressed as the difference $Ts_{\text{off-nadir}} - Ts_{\text{nadir}}$ between off-nadir and nadir observations of temperature in a given zenith/azimuth viewing direction. This anisotropy, also referred to as effective anisotropy by Voogt (2008), is defined for spatial scales larger

* Corresponding author.
E-mail address: lagouarde@bordeaux.inra.fr (J.-P. Lagouarde).

0034-4257/$ – see front matter © 2011 Elsevier Inc. All rights reserved.
doi:10.1016/j.rse.2011.06.022

than the dominant surface structure (e.g. building dimensions) so that it represents the effects of the three-dimensional surface rather than the non-lambertian behaviour of individual surfaces (Voogt, 2008). The surface temperature Ts can be defined in several ways, resulting in different possible characterizations of the anisotropy. In this paper we shall unequivocally consider the directional brightness, or simply 'brightness' temperature, according to the definition of Norman and Becker (1995), when dealing with the measurements. The definition of the modelled temperatures is not so clear: they are computed solving energy budget equations, and therefore appear as 'equilibrium' temperatures. This will be discussed in detail in the text.

During daytime, because of thermal contrasts between shaded and sunlit facets within canopies, differences between oblique and nadir measurements may reach up to 10°C depending on the relative positions of the Sun and sensor: the directional anisotropy displays characteristic patterns with intense 'hot spot' effects (maximum temperature when the surface is observed in the anti-solar direction), as described by several authors (Lagouarde et al., 2010; Lagouarde and Irvine, 2008; Soux et al., 2004; Voogt, 2008).

The presence of nighttime urban anisotropy, forced by cooling differences associated with urban surface structure and materials was first suggested by Roth et al. (1989) and briefly illustrated in Voogt and Oke (2003; Fig. 4) but no detailed study of the nighttime directional anisotropy has been performed until now. The distribution of the temperatures of the facets within the urban canopy depends on coupled energy and radiative transfer processes. At night, heat conduction processes that depend on thermal inertia of materials and internal heating of buildings, together with the processes governing the net loss of longwave radiation are expected to govern the anisotropy. This marks a substantial difference from the daytime case that is dominated by differences in the solar loading on particular facets of the urban surface. This paper focuses on nighttime anisotropy and follows our previous work devoted to daytime anisotropy in the same city (Lagouarde et al., 2010). The research was performed as part of the CAPITOUL project over the city of Toulouse in 2004–2005 (Masson et al., 2008). In this paper we briefly review the observational protocol used with the airborne TIR imager, the details of which are provided in Lagouarde et al. (2010), and then present the results obtained during 3 nights in autumn and winter conditions. An anisotropy modelling approach is then described: it is based on the combination of a 3D model providing the actual urban structure with canyon street energy models computing the distribution of the temperatures of the canopy facets. The results of the simulation are evaluated against the observations and the sensitivity of the modelled anisotropy to possible uncertainties arising from the urban canopy geometry and radiative and thermal surface parameters are discussed. An extension of the results is finally proposed using the model to assess the time evolution of the anisotropy throughout the entire night.

2. Experimental

2.1. Experimental protocol

Details of the experimental protocol have already been described in previous papers (Lagouarde et al., 2010; Lagouarde and Irvine, 2008); its main features are summarised here for clarity. The TIR directional measurements were performed using 2 airborne TIR cameras placed aboard a small twin-engine aircraft Piper Aztec PA23 flown by the SAFIRE group (http://www.safire.fr/ Service des Avions Français Instrumentés pour la Recherche en Environnement). The 2 cameras, M740 (INFRAMETRICS [1]) and SC2000 (FLIR [1]), were equipped with 75×59° wide angle and 24×18° lenses respectively and placed aboard the aircraft with backward inclinations of 9.5 and 50°. After having installed an additional filter on the SC2000 camera with a band pass cut off at 13 μm, both instruments had quite similar spectral responses between 7.5 and 13 μm. The flight altitude was 2000 ft (above sea level), which corresponds to about 460 m above ground for the centre of Toulouse. The spatial resolutions ranged between 2.5 m (nadir) and 6.2 m (50° zenith viewing) for the M740 and between 1.5 and 3.0 m for the SC2000 (for 48 and 62° zenith viewing angles respectively). The sizes of the images are 257×370 and 240×320 pixels for the M740 and SC2000 respectively. Fig. 1 shows the corresponding areas seen at ground. The aircraft speed was 70 ms^{-1} and the images were acquired at 1 Hz (M740) and 4.3 Hz (SC2000). Each pixel of the images corresponds to particular viewing zenithal and azimuthal angles θ_v and φ_v (whose computations can be found in Lagouarde et al., 2000). The partial overlapping of the FOV of the two instruments is used for intercalibration of the recorded images.

The protocol of measurements consisted of a set of several short flight lines flown in opposite directions all crossing at the city centre. For nighttime, the flight lines were oriented N↔S, W↔E, NW↔SE and NE↔SW. Radiosoundings were simultaneously performed by Météo France to provide atmospheric profiles of temperature and humidity for use with the LOWTRAN 7 model (Kneisys et al., 1988) to determine atmospheric corrections for the thermal measurements. Measurements of surface temperature at ground level were also collected simultaneously to the flights by three groups using hand-held TIR radiometers (Minolta/Land Cyclops Compac 3 [1]) along 2 streets close to the central site, viewing walls, streets and pavements. A few measurements over roof samples were also collected.

The reader is referred to the papers of Lagouarde et al. (2000, 2004) which describe the data processing in detail. Combining all the images acquired along the 8 flight lines allows one to generate the anisotropy $T_{b\ off\text{-}nadir} - T_{b\ nadir}$ averaged by 1° steps on and in all azimuthal viewing directions φ_v (referred to North) and for zenithal view angles θ_v (referred to nadir viewing) up to 60°. No correction for pitch and roll angles of the aircraft were performed, but the excellent flight conditions at night led us to consider the accuracy on the θ_v and φ_v angles as being within ±2°. The same (θ_v, φ_v) viewing geometry

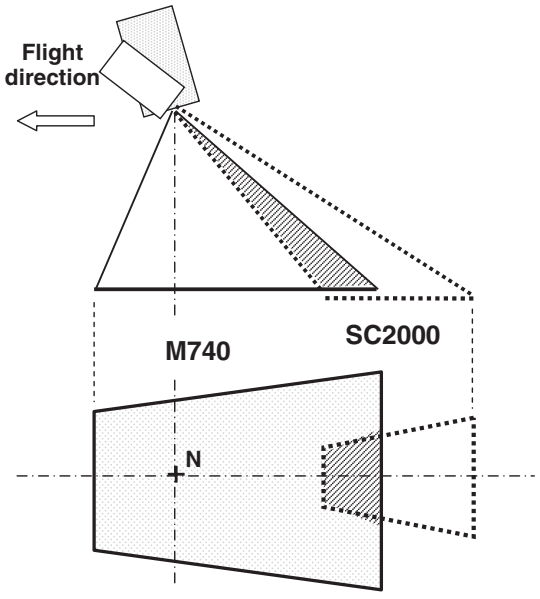

Fig. 1. Principle of angular measurements: schematic of instrumental setup aboard the aircraft with corresponding areas seen at ground level. For a 460 m flight height above ground, the approximate size of the areas is 720×440 to 570 m and 490×180 to 300 m for the M740 and SC2000 cameras respectively. The dashed areas indicate the overlapping of the FOV of the 2 cameras and the corresponding area at ground. N corresponds to the nadir of the aircraft.

[1] Trade name and company are given for the benefit of the reader and do not imply any endorsement of the product or company by the authors.

can be met for different pixels along different flight lines. Consequently, the ensemble of measurements available for a given (θ_v, φ_v) during a set of flight lines corresponds to different locations on the ground and to different acquisition times. They are prone to noise due to both heterogeneity of the site and to natural temporal fluctuations of surface temperature related to turbulence. The acquisition protocol, together with the processing of data, allows a 'spatio-temporal' smoothing of the retrieved directional anisotropy over the entire study area. It significantly contributes to the robustness of our results.

As little is known about large-scale directional emissivity (Becker and Li, 1995; Li et al., 1999), we only derived brightness temperatures (T_b) at ground level from our measurements. They correspond to the black body equivalent temperatures derived from the overall radiation from the ground (in the spectral window of the sensor) which results from both the TIR emission and the reflection of the ambient radiation. We therefore consider the emissivity to be lambertian and equal to unity in this work.

The measurements were performed during several intensive operation periods (IOP) during years 2004 and 2005 of the CAPITOUL experiment (Masson et al., 2008). In this paper we focus on 3 nighttime flights performed in autumn (October 5th, 2004) and winter conditions (February 24th and 25th, 2005) for which anthropogenic effects (heating of buildings) are expected to have more impact (Pigeon et al., 2007) and daytime solar zenith angles are relatively large. The characteristics of the flights and the times of measurements are provided in Table 1. Flight times were chosen around 22:00 and 23:00 UTC; it was late enough after sunset (i) to eliminate possible differences of temperature resulting from the previous afternoon in relation with thermal inertia, and (ii) to have prevailing radiative cooling processes only. At the same time, it was early enough to avoid possible development of fog close to the surface. Average air temperature and wind speed measured during the flights on a central site mast at 47.5 m above ground are also indicated in Table 1.

2.2. Study area

Using the PhotoExplorer 3D product of IGN (http://www.ign.fr/), a visual interpretation of the air photos and our knowledge of the city, we determined a study area (about 2×3 km) that we considered to be representative of the old Toulouse city centre (Fig. 2). This area on which the directional anisotropy has been integrated is densely built and rather homogeneous. Most of the buildings are ancient ones built with red brick walls (average height 15 m) and covered with tiled roofs; a few modern ones exhibit roofs covered with gravel and aluminium composites. Streets are oriented in all directions and display a large variety of widths. A few large squares and open spaces can be found. The fractional area of vegetation is low, with trees concentrated along a few wide 'boulevards' only. In the vicinity of the CAPITOUL central measurement site situated close to the Capitole square in the very centre of the city the plan area fractions of roofs, roads and vegetation are 0.54, 0.38, and 0.08 respectively (Masson et al., 2008).

2.3. Results

The results of the airborne observations are given in Fig. 3 (left side). They are synthesised in polar plots in which the radii correspond to the azimuthal viewing direction and the concentric circles indicate the zenithal viewing angles. The differences between off-nadir and nadir brightness temperatures are colour-coded. The 'toothed wheel' aspect of the polar plots presented is easily explained by the fact that the experimental setup makes possible to document all the φ_v directions only with the M740 camera.

The polar plots reveal that the anisotropy is slightly growing from nadir but remains very low at the 3 dates and does not exceed 1°C for $\theta_v < 50°$. Moreover no systematic effect of azimuthal direction can be observed. The variability around 60° θ_v angles for the two February dates is small, with a standard deviation of 0.4°C when all azimuthal directions are combined (compared with the 1°C accuracy of the measurements). If carefully examined, the polar plots sometimes reveal some structures corresponding to large strips about 30° wide in θ_v angle, which is half the transverse FOV of the wide angle M740 lenses: each strip corresponds to a flight line, and these artefacts can easily be explained by natural time fluctuations of surface temperature between the different lines flown successively, or by heterogeneities in landuse possibly inducing small systematic differences in temperature between flight lines. As an example they are illustrated by the linear features observed in the NS direction in the polar plot of 0443 flight. The mean dependence of anisotropy with θ_v has therefore been derived by averaging all the φ_v directions for each of the 3 flights. The result (Fig. 4) illustrates the increase of anisotropy with θ_v. The gentle undulations that can be seen correspond to the artefacts noted above. The anisotropy effects are similar for the two consecutive winter nights, whereas they appear somewhat smaller for the fall night. The reason is likely to be found in differences in micrometeorological conditions, such as wind speed and atmospheric downward longwave radiation which have important impacts on nocturnal cooling of surfaces. These will be analysed further in Section 5.1.

As expected, the absence of azimuthal dependence can be explained by the acquisition time of night images (around 21:00 or 22:00 UTC) which is likely to be too late to observe any residual effect

Fig. 2. Aerial photograph of the city centre of Toulouse: 3500×4400 m sample of IGN (Institut Géographique National) panchromatic image of June 24, 1998 (courtesy of IGN). The white continuous line approximately corresponds to an area of the old city centre that has been taken as the sampling area for extracting TIR directional anisotropy. The circle indicates the position of the central site.

Table 1
Characteristics of the nighttime flights performed over Toulouse (the dates refer to the end of flights in local time).

Flight	Date	Time (UTC)	AGL height (m)	Ta (°C)	U (ms^{-1})
0443	October 5th, 2004	22:41–23:17	475	20.4	4.0
0510	February 24th, 2005	21:46–22:43	450	1.1	1.5
0512	February 25th, 2005	21:56–22:50	460	2.4	2.6

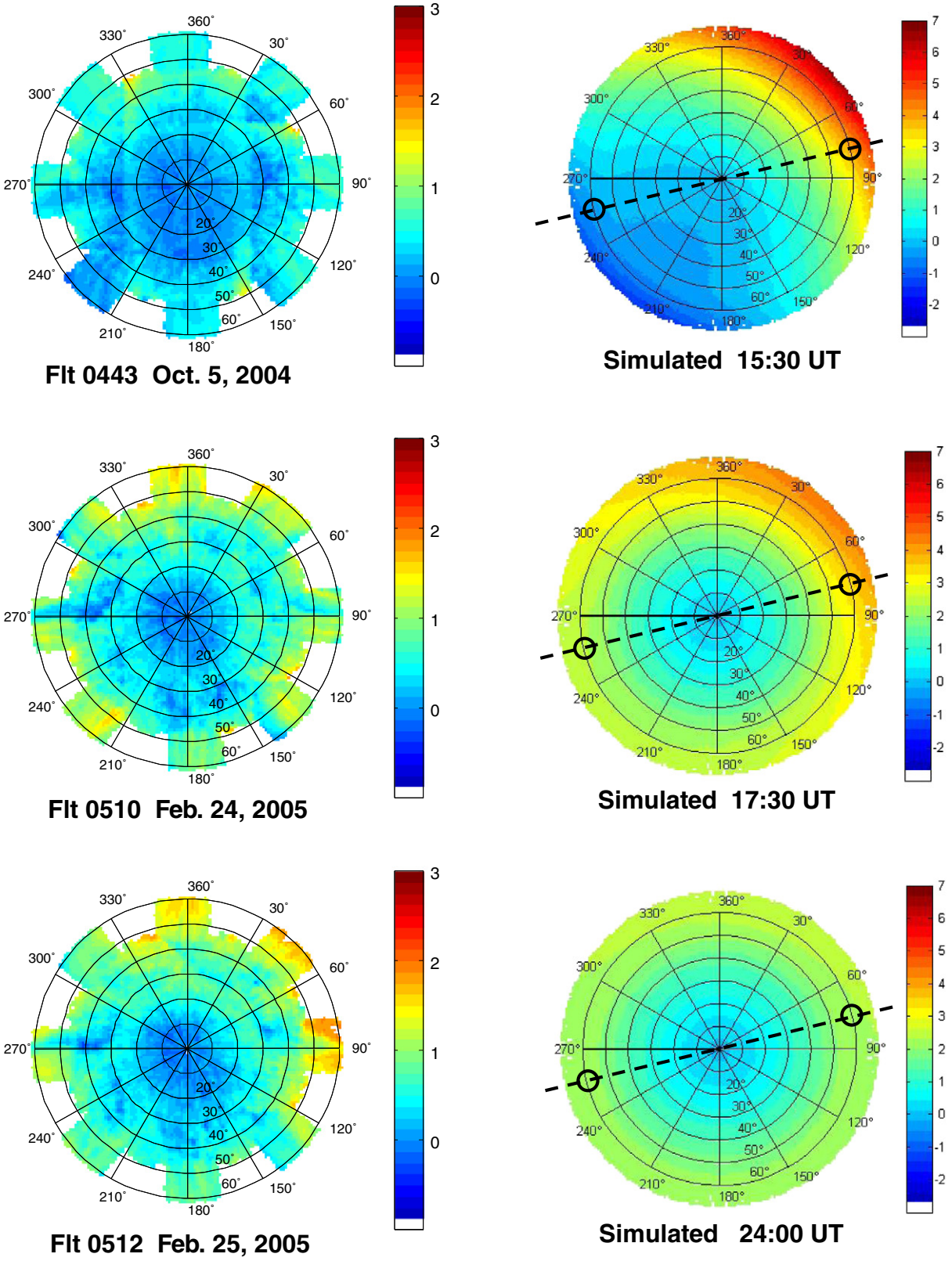

Fig. 3. Left: polar plots of the measured TIR directional anisotropy over Toulouse for 1 autumn night (2004 October 5th around 23:00UTC, for flight 0443) and 2 winter dates (2005 February 24th and 25th around 22:15 and 22:30UTC for flights 0510 and 0512 respectively). For comparison purposes, the same colour scale has been used for the difference between oblique and nadir brightness surface temperatures. The radii correspond to the azimuthal viewing directions φ_v and the concentric circles indicate the zenithal viewing angles θ_v. Right: directional anisotropy simulated at 15:30, 17:30, and midnight on February 25th, 2005 (corresponding to 0512 flight) shows that azimuthal heterogeneity vanishes between the end of the afternoon and the beginning of the night (see text). The black dotted line corresponds to the solar plane at sunset, and the 2 black circles refer to the comparison of anisotropy performed for illustrating thermal inertia effect (see Section 5.2 and Fig. 17).

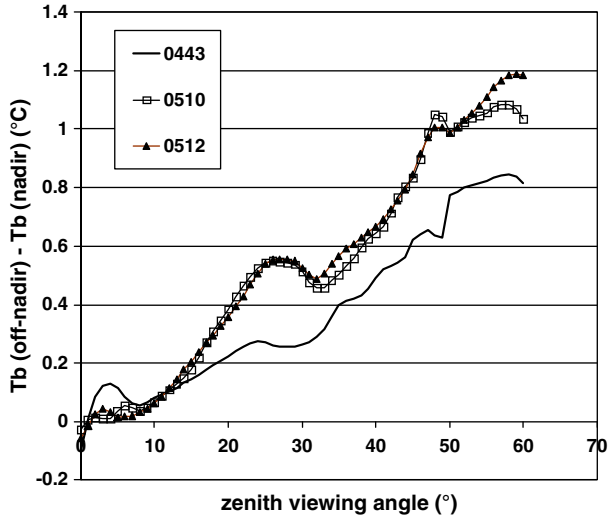

Fig. 4. Dependence of the night directional anisotropy (azimuthally averaged) retrieved from airborne measurements with the zenith viewing angle over the city centre of Toulouse for fall (0443) and winter (0510 and 0512) flights.

of the strong anisotropy observed during afternoon. Images acquired just after sunset (occurring at 17:27 and 17:31 UTC for October and February dates respectively) or at the beginning of the night would likely have revealed an azimuthal dependence on the anisotropy due to warmer temperatures on the latest sunlit west walls, and with the thermal inertia of the buildings. This point will be examined in details and confirmed further, in Section 5.2.

3. Modelling

3.1. Principle of the simulation

In the absence of any atmospheric effect, the radiance received by a TIR sensor aimed at a complex surface in a given viewing direction results from the aggregation of the TIR radiance $L_k(\theta_v, \varphi_v)$ coming from the ensemble of facets of the canopy seen in the FOV of the instrument. The facets may differ by the materials, surface properties, orientations, etc. k being the facet index, we have:

$$L(\theta_V,\varphi_V) = \int_{k\in FOV} L_k(\theta_V,\varphi_V) \quad (1)$$

$L_k(\theta_v, \varphi_v)$ includes both the emitted thermal radiation from the facet and that reflected from the surroundings. A brightness temperature can directly be retrieved from the integrated radiance $L(\theta_v,\varphi_v)$. If we consider the radiometric surface temperatures, the retrieval is much more complex, because it also requires an aggregation scheme for the emissivity. In what follows, we shall consider brightness temperatures only.

The simulation strategy is similar to that used for daytime conditions (Lagouarde et al., 2010) and even simpler because of the absence of sunlit areas. Instead of being performed at the facet scale (by aggregating individual facets) as in Eq. (1), the aggregation is performed on a limited number of surface types also referred to as 'class' in what follows. Three surface types, walls, roofs and ground, composing the canopy are considered in this paper:

$$T_b(\theta_V,\varphi_V) = \left[\sum_{i=1}^{3} A_i(\theta_V,\varphi_V)\left[T_{b,i}(\theta_V,\varphi_V)\right]^4\right]^{1/4} \quad (2)$$

where $A_i(\theta_v,\varphi_v)$ and $T_{b,i}$ (θ_v,φ_v) are the overall fraction of each class and its averaged brightness temperature in the viewing direction (θ_v,φ_v) respectively. Eq. (2) assumes that all the directionality of the temperature can be split in two terms: A_i represents the effect of geometry of the scene whereas the variability of the temperatures of each facet type in relation with local energy and radiative transfers is introduced through the $T_{b,i}$ term.

The aggregation scheme used in Eq. (2) is based on the conservation of the Stefan-Boltzmann TIR radiance. This simple scheme was selected after having performed a numerical study comparing it against more realistic aggregation schemes based on the integration of the actual radiances measured in the spectral window of the TIR cameras (Lagouarde et al., 2010). It is all the more justified in our case as the $T_{b,i}$ display only small variations in nighttime conditions.

3.2. Determination of the A_i fractions

The A_i fractions were calculated from images of the urban canopy generated in each viewing direction using the POV-Ray (http://www.povray.org) ray tracing software. The required 3D information on the canopy structure was extracted from the 3D database of the city made available for the CAPITOUL project by the administrative authorities (Mairie) of Toulouse. Each of the three class directional fractions was simply calculated by adding the corresponding shaded and sunlit ratios on an already available dataset of daytime images simulated in the framework of the previous study of daytime anisotropy. These had been generated in every studied viewing direction with the intent of generating simplified images that displayed strong contrasts to ease the discrimination between the 6 classes: sunlit/shaded ground, sunlit/shaded walls and sunlit/shaded roofs. For this purpose, the scene was illuminated by a distant point source simulating the Sun (with no diffuse ambient radiation), and arbitrary surface properties (reflectance, colours, etc.) were given to the facets. The whole scene was viewed with parallel beams in a single direction (stated as 'orthographic' in POV Ray software). A 2.5 m resolution justified by a previous study of its sensitivity on the A_i determination was chosen and 1000×1000 pixel images were generated. For details the reader is referred to Lagouarde et al. (2010).

The POV-Ray simulations were performed with the 3D surface model defined on the test area shown in Fig. 2 only, and no canopy outside of it. To avoid errors due to edge effects, a 30 m wide buffer was removed from the test area prior to calculating the A_i fractions.

The simulations were repeated by varying the viewing direction between 0 and 60° in 5° steps for θ_v, and between 0 and 350° in 10° steps for φ_v. A final interpolation was performed to generate the A_i fractions at 1° intervals. Fig. 5 displays the polar plots of the fractions of each class in the different viewing directions. The ground fraction is logically a maximum for nadir viewing for which it is equal to the complement of the plan area ratio (defined as the built surface fraction), 0.46; it decreases when zenithal viewing angle increases because of the masking of the walls, to reach about 0.14 at $\theta_v = 60°$. The fraction of walls varies between 0 at nadir (for which no vertical wall can be seen) and 0.42 at 60° zenith angle. Roofs are visible in any viewing direction and, due to their low slope, their fraction varies only in a limited range, between the plan area ratio, 0.54, at nadir and 0.45 at $\theta_v = 60°$. Moreover all polar plots in Fig. 5 display a radial symmetry, which indicates that no prevailing direction exists in the structure of the urban canopy.

3.3. Determination of the $T_{b,i}$

Two approaches have been tested for determining the mean directional temperatures by surface class $T_{b,i}$ (θ_v,φ_v). They differ by the urban surface canopy parameterization model used; in the first approach the TEB (Town Energy Budget) model developed at Météo France is used, and in the second, SOLENE developed at CERMA Nantes.

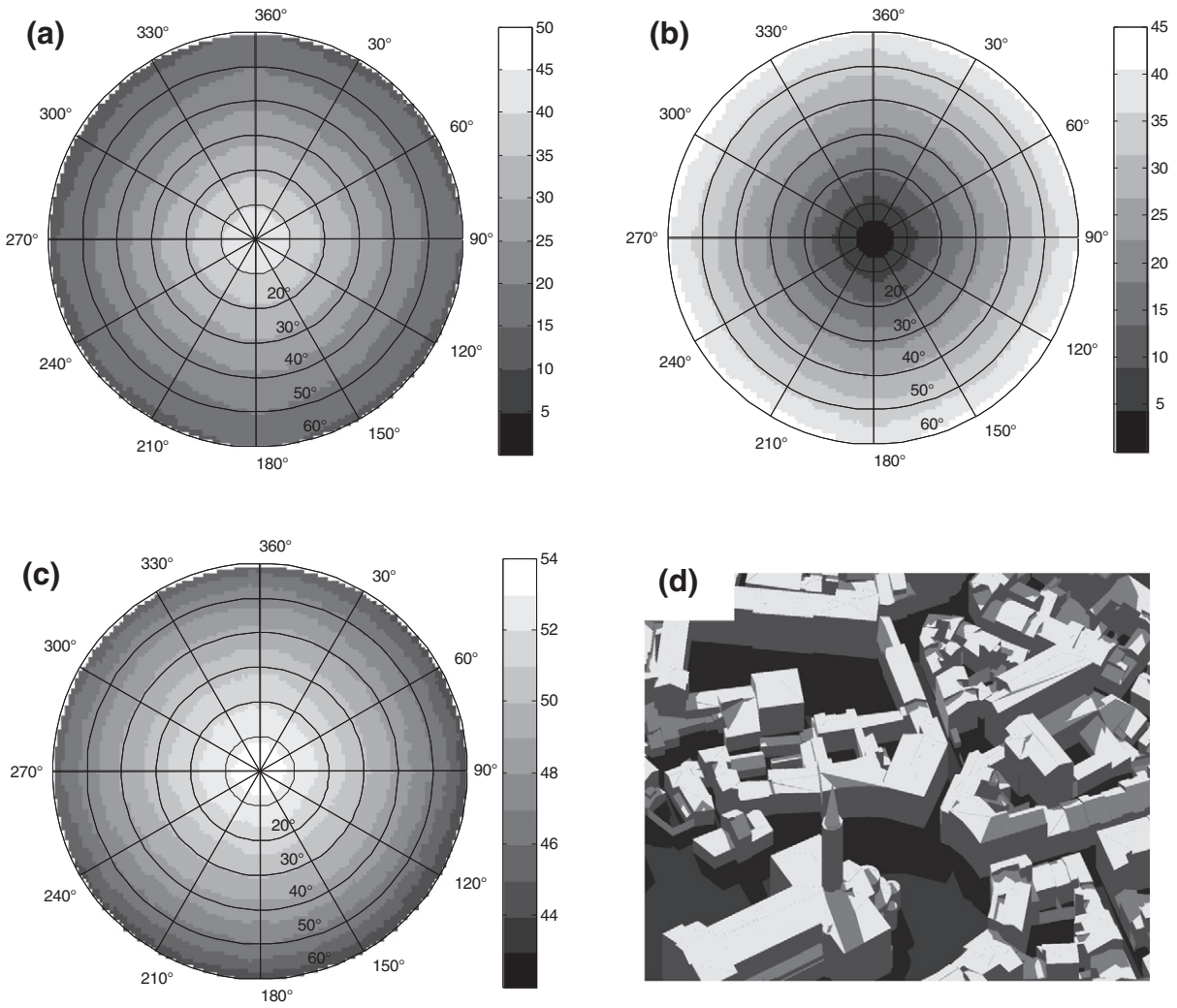

Fig. 5. A_i fractions (in percent) for streets (a), walls (b) and roofs (c). Example of POV-Ray generated image of the S^t Sernin Church district from the 3D database (d).

3.3.1. TEB approach

The Town Energy Balance (TEB) model (Masson, 2000; Masson et al., 2002) simulates the local-scale urban surface energy budget for urban areas. TEB computes the conduction and convection (heat and water) fluxes together with radiative exchanges. For this purpose it considers a very simple representation of the urban canopy based on the street canyon. Each of the three components of the canyon – road, walls and roofs – is processed globally without any discretization, so that the model cannot describe temperature variations within these surfaces (for instance the partition between sunlit and shaded parts during daytime). Moreover roofs are assumed to be flat for simplification. The radiative long wave transfers are based on form factor computations, and only one re-emission is taken into account. The geometrical structure of the city is introduced assuming that any road orientation is possible and that all exist with the same probability, which leads to averaging of all directional variables over 360° in the computations. TEB was developed to be coupled with an atmospheric model, but it can also be forced by local meteorological data. It solves the energy budget equations for each component of the canyon street using schemes and parameterizations described in detail by Masson (2000), and in addition to the fluxes it also computes their surface temperatures. TEB has been validated both for fluxes and surface temperatures on 2 cities (historic core of Mexico City and light industrial site in Vancouver) in dry and hot conditions by Masson et al. (2002) and over Marseille in summer by Lemonsu et al. (2004); more recently it has been validated over the dense urban area of Toulouse by Pigeon et al. (2008) in fall and winter conditions, and over Montreal (Canada) by Leroyer et al. (2010) and Lemonsu et al. (2010).

TEB computes what might be called an 'equilibrium surface temperature' that is the temperature associated with the solution of the surface energy balance. As a matter of fact this equation mixes temperatures obeying different definitions in its different terms: in the radiative terms, the temperature appears to be a 'hemispherical radiometric' temperature, whereas it is clearly an 'aerodynamic' temperature in the expression of the sensible heat flux, according to the definitions of Norman and Becker (1995). The term 'equilibrium temperature' therefore seems to be the more appropriate (Huband and Monteith, 1986). This temperature differs from the brightness temperature. Contrary to the aggregation of brightness temperatures that has a physical meaning because it comes to add energy fluxes, the aggregation of equilibrium temperatures is more difficult to justify. This has nevertheless been done using Eq. (2) to derive so-called 'directional ensemble equilibrium temperatures' on which we studied the resulting anisotropy. Elements of justification of this approach will be given further in Section 4.2.4.

3.3.2. SOLENE approach

Initially designed for simulating sunshine, natural lighting and thermal radiation over buildings or urban blocks for architectural projects, the SOLENE software (http://www.cerma.archi.fr/CERMA/Expertise/solene/) has recently been modified by introducing energy transfer processes within it with the objective of simulating surface

temperatures and convective and conductive fluxes (Henon, 2008). It is based on a realistic description of the canopy structure using a geometrical 3D model made of facets to which surface radiative and thermal properties are assigned. Whereas TEB provides one unique temperature per class independently of the viewing direction, the SOLENE approach allows one to take into account the heterogeneity induced by the geometry of the canopy in a more realistic manner.

The components of the radiative budget of each facet at any time step are first modelled using a radiosity approach in the solar domain and assuming only one reflection in the thermal domain. The surfaces are assumed to be dry and the latent heat flux is neglected. The sensible heat flux is classically estimated using a bulk transfer equation. In the version of SOLENE used in this paper, a crude approximation of the forcing constant values for transfer coefficients was used. More recent versions of the model now include a parameterization of the wind profile above and within the canopy. The storage heat flux is estimated using the heat transfer equations through walls, ground and roofs which are represented by two-layer systems with different thicknesses, heat capacities and thermal conductivities. An aerodynamic surface temperature is finally computed by solving an energy budget equation for each facet. Additionally for our purpose the brightness temperature was simultaneously estimated using the longwave terms of the radiative budget. The model has been validated (Henon, 2008; Hénon et al., 2011) against flux data collected during two experimental campaigns which took place over Marseille (ESCOMPTE) in 2001 (Cros et al., 2004; Mestayer et al., 2005) and Toulouse (CAPITOUL) in 2004–2005 (Masson et al., 2008). Hénon et al. (2009a,b) recently also presented satisfactory comparisons of canopy brightness temperatures simulated by SOLENE at 1 m resolution against airborne observations over a 18 000 m² urban study area within the centre of Toulouse.

For estimating the mean directional temperatures by class $T_{b,i}(\theta_v,\varphi_v)$, we followed the approach previously developed for modelling daytime TIR anisotropy (Lagouarde et al., 2010) in which the city is represented by an ensemble of canyon streets. Computing time limitations made us choose this simplified representation of the city. It assumes the structure of Toulouse to be homogeneous, with streets in all directions. We considered it was equivalent to 18 streets with orientations in 10° steps from North. The complementarity between the opposite sides of the canyon means that it is sufficient to assess all the possible street configurations in the city and to provide a representative sampling of the temperatures of all the facets. The surface temperatures of the canyon streets were integrated in every (θ_v,φ_v) viewing direction to finally derive the resulting directional brightness temperature $T_{b,i}(\theta_v,\varphi_v)$. In this process all the streets were given the same weight. The reader is referred to the Appendix A for more details on the integration process.

4. Modelling results

4.1. Assessment of the quality of TEB and SOLENE simulations

The TEB simulations were performed by Météo France for a small area within a 500 m radius circle around the reference energy budget station of the CAPITOUL experiment, close to the centre of Toulouse. The details of the simulations and the parameters used (referred to as P0 in what follows and in Table 2) are given in Pigeon et al. (2008). The building height H and street width W of the canyon street are 15 and 10 m respectively (this geometry being referred to as G0 in this paper). Figs. 14a and 15a presented further in the paper display the time evolution of the temperatures of roofs, walls and ground for the two study periods: 2004 fall (flight 0443) and 2005 winter (Flights 0510 and 0512). The February 24th and 25th nights yield similar results, while the temperature contrast between roofs and other elements is smaller for the October 5th night.

The SOLENE simulations have been performed using 2 sets of input data:

- For comparison purposes, the geometry and parameters used in the TEB simulations (G0, P0) were first used. To preserve the correct plan area ratio of 0.54, and to cope with their 20° slope, the length of the roof on each side of the street has been set at 6.2 m.
- Second, simulations have been performed with the data used in a previous study of the TIR daytime anisotropy and described in Lagouarde et al. (2010). The geometry of the canyon street here is an average representative of the entire study area (Fig. 1) over which the airborne measurements have been integrated: H = 5 m, W = 17 m, with a 10.6 roof length (G1 geometry). The thermo-radiative parameters (referred to as P1) are those which were obtained by fitting SOLENE against daytime ground measurements. They are given in Table 2 together with P0.

Fig. 6 helps to assess the consistency of TEB and SOLENE simulations. It illustrates the surface temperature profiles across the street for the 3 simulations (TEB P0-G0, SOLENE P0-G0 and SOLENE P1-G1) for flights 0443 and 0512. The simulations are quite consistent. All display the lowest temperatures for roofs, which is easily explained by the fact they 'see' most sky and are subject to maximum radiative losses. As they radiate towards each other and receive emitted longwave radiation from street, the walls are the warmest surface in the canyon. For the same reasons, the street display intermediate temperatures. Nevertheless these differences are not just radiatively driven, but they are also governed by combined differences in the thermal properties of surfaces: the roofs have the smallest heat capacity whereas walls and roads have a much greater heat capacity and store of heat from which to draw upon through the night. We also see in Fig. 6 that, in contrast to TEB, SOLENE can simulate the variability of the temperature across the canyon facets: in particular the increase of temperature on both sides of the street and at the base of the walls is related to multiple reflections and more efficient radiation trapping at the bottom of the canyon.

The simulated surface temperatures averaged by class are given in Table 3 together with ground measurements performed simultaneously with the flights by several teams equipped with handheld infrared thermometers. The teams operated in several streets of different orientations close to the central site (MONOPRIX building). Sets of measurements within short time intervals were acquired at different locations along the streets, with the scope of integrating both the natural temporal fluctuations of the surface temperature (in relation with micrometeorological conditions) and its spatial variability within a given class. The standard deviations of the ground measurements are

Table 2
Sets of thermo-radiative parameters P0 and P1 used in the SOLENE simulations: characteristics and thermal properties (thermal conductivity λ and capacity c_p) of the two-layer model for roofs, walls and streets. The prescribed emissivity and albedo are also given.

Surface type	Layer	Material	Thickness (m)	λ ($Wm^{-1}K^{-1}$)		c_p 10^6 J $m^{-3}K^{-1}$	ε	a
				[P0]	[P1]			
Roof	1	Tile	0.06	1.15	1.15	1.58	0.90	0.15
	2	Insulating material	0.15	0.2	0.04	2.20		
Wall	1	Red brick	0.06	1.15	0.6	1.58	0.92	0.15
	2	Red brick	0.24	1.15	0.6	1.58		
Street	1	Tar	0.05	0.82	0.82	1.74	0.95	0.08
	2	Soil	0.2	2.1	2.1	2.0		

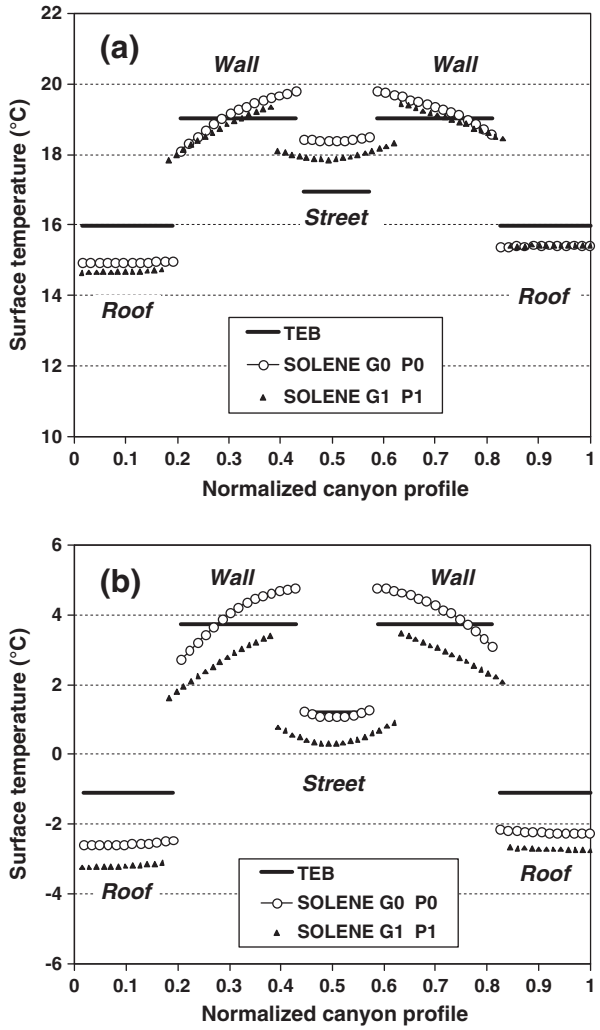

Fig. 6. Comparison of street temperature profiles simulated with TEB and SOLENE for flights 0443 (a, fall) and 0512 (b, winter). The X axis corresponds to normalised i index shown in Fig. 18b.

also provided in Table 3. Problems of accessibility to the roofs made it difficult to obtain an extensive sampling of roof surfaces; measurements were performed at 2 locations only for each flight, both given in Table 3. The analysis of the table reveals that the agreement between all simulations and measurements, within a 2° range, is pretty good, especially considering the season and the relative accuracy of the hand held IRTs under these conditions. One also notices that, despite possible differences between absolute values, the relative differences between the temperatures of the different surface types agree quite well: this is particularly important as these govern the directional anisotropy amplitude. This comparison exercise, which we do not consider to be a formal validation of the model, provided confidence in the quality of the models and their suitability to our objectives.

Table 3
Comparison of the simulated and ground measured temperatures (with standard deviation) by surface type for the 3 flights 0443, 0510 and 0512. All measurements in °C.

Flight	Surface type	TEB	SOLENE G0 P0	SOLENE G1 P1	Ground measurements
0443	Roof	16.0	15.2	14.9	15.5 (0.9)
					15.4 (2.9)
	Wall	19.0	19.2	18.8	19.4 (0.9)
	Street	16.9	18.4	18.0	18.9 (1.0)
0510	Roof	−2.2	−2.7	−4.0	−3.9 (2.6)
					−4.1 (1.7)
	Wall	3.2	4.0	2.1	2.3 (1.2)
	Street	0.6	0.9	−0.2	1.2 (1.0)
0512	Roof	−1.1	−2.1	−3.0	−4.7 (1.6)
					1.4 (1.4)
	Wall	3.7	4.2	2.7	2.8 (1.5)
	Street	1.2	1.4	0.5	1.2 (1.0)

4.2. Simulation of the TIR nighttime anisotropy

4.2.1. Comparison against experimental measurements of anisotropy

The comparison between the measured and simulated anisotropy presented in Figs. 7 to 9 reveals generally good agreement for the 3 flights. The error bars correspond to ±1 standard deviation of the azimuthal values of the retrieved anisotropy for a given zenith viewing angle. Most simulated values fall within the range of these error bars. Moreover for zenith viewing angles less than 50°, the differences between modelled and measured mean values remain lower than 0.4°C. This is a very good result considering that the accuracy of the TIR cameras used, which also contributes to the uncertainty on measurements, is about 1K. Despite the assumption of flat roofs, TEB-based simulations perform well. This may be related to the low slopes of the roofs in our Toulouse study area, but would need further confirmation for other cities.

The simulations confirm that the nocturnal TIR directional anisotropy is rather low, at least in the middle of the night at the time of the measurements. The anisotropy is smaller for the October 0443 flight, which is consistent with the reduced thermal contrasts between roofs, streets and walls described in Section 4.1. The evolution of the anisotropy throughout the night and the possible impact of the thermal inertia of buildings at the beginning of the night will be discussed further in Section 5.

In the SOLENE simulations, we combined two canyon street geometries and two sets of thermal parameters chosen to be representative of the city centre (around the central MONOPRIX site) and of a larger study area. Performing systematic sensitivity tests to geometry and input thermo-radiative parameters is a significant task beyond the scope of this paper. Here we have performed a few additional simulations to evaluate the impact of the choice of the geometry (G0 or G1) and parameters (P0 or P1) separately on the modelled anisotropy.

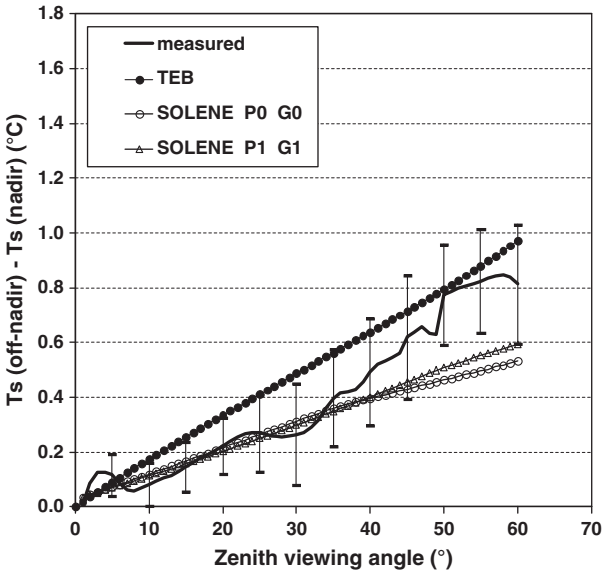

Fig. 7. Comparison between measured and simulated TIR anisotropy for flight 0443 (October 5th, 2004). For each zenith viewing angle, the values have been averaged on the 0–360° range of azimuthal directions, with error bars representing ±1 standard deviation.

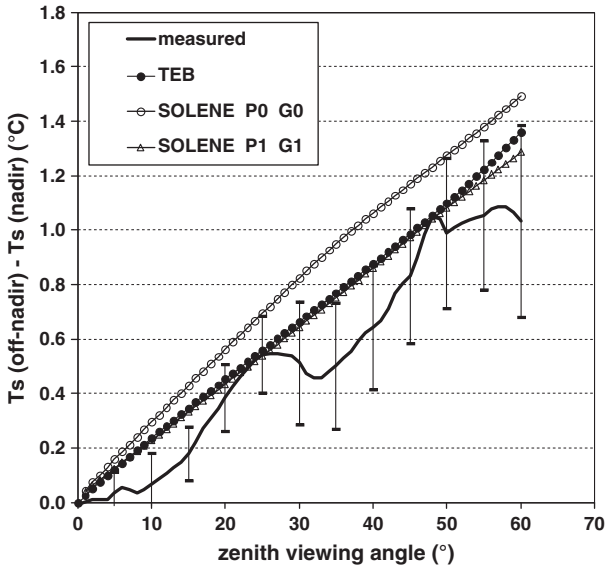

Fig. 8. Same as Fig. 7 for flight 0510 (February 24th, 2004).

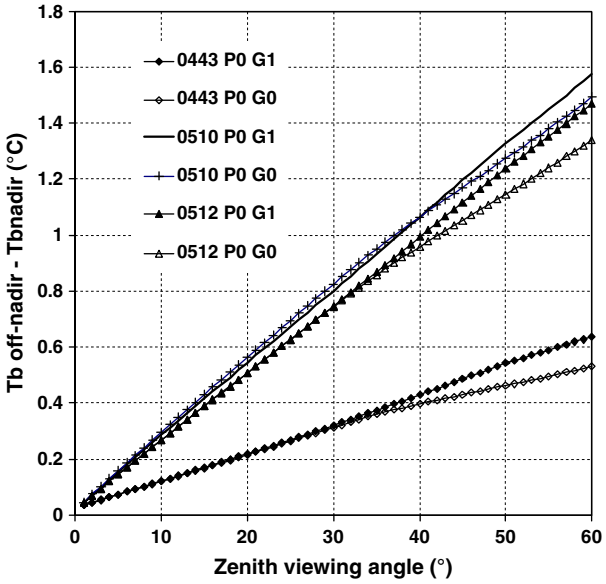

Fig. 10. Impact of the uncertainty of the canyon street geometry on the anisotropy determined with the SOLENE approach.

4.2.2. Sensitivity to the canyon street geometry

The sensitivity to the geometry has been evaluated using the same P0 set. The results (Fig. 10) show no difference for $\theta_v < 35°$, and a small increasing divergence after. The 35° angle roughly corresponds to that for which the street is completely masked by the neighbouring walls for a G0 canyon street oriented perpendicularly to the viewing direction. In this configuration it also corresponds to the angle from which none of the walls can be seen entirely. This suggests that the discrepancy beyond 35° could be related to a larger participation (for the G1 case) of walls – which are the warmest elements in the canopy – to the integrated directional temperature. The overall anisotropy is nevertheless not significantly affected, with differences not exceeding 0.1°C.

4.2.3. Sensitivity to the thermal parameters

The comparison of the anisotropy simulations with thermal parameter sets P0 and P1 and using the same canyon profile G1 is presented in Fig. 11. The sensitivity to the thermal parameters is a little larger than to the geometry. It nevertheless remains limited to 0.3K for the most oblique viewing directions (at $\theta_v = 60°$).

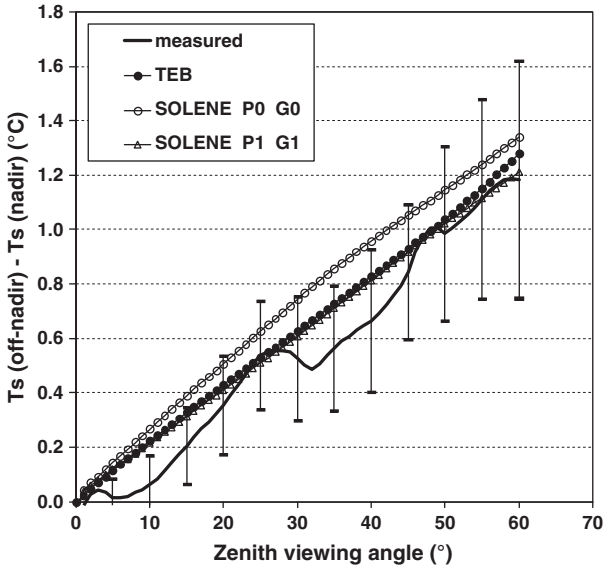

Fig. 9. Same as Fig. 7 for flight 0512 (February 25th, 2004).

Over the zenithal viewing range 0–45° often most used for limiting the impact of atmospheric effects, the combined sensitivity to thermal parameters and uncertainties on the effective canyon street geometry representing the urban canopy structure do not exceed 0.2°C in our simulations. It is small enough to confirm the directional variations of anisotropy we observed and modelled.

4.2.4. Impact of the nature of the facet temperature used

In their standard version, both TEB and SOLENE provide equilibrium temperatures estimated by solving the energy budget equation for each surface type or facet. As described in Section 3.3.2, a brightness temperature was additionally computed with SOLENE. This made it possible to evaluate the impact of the surface temperature definition, 'equilibrium' or 'brightness', on the anisotropy. The difference of anisotropy retrieved when using the two temperature types are not significant and reach no more than 0.05°C at 60° zenith viewing angle.

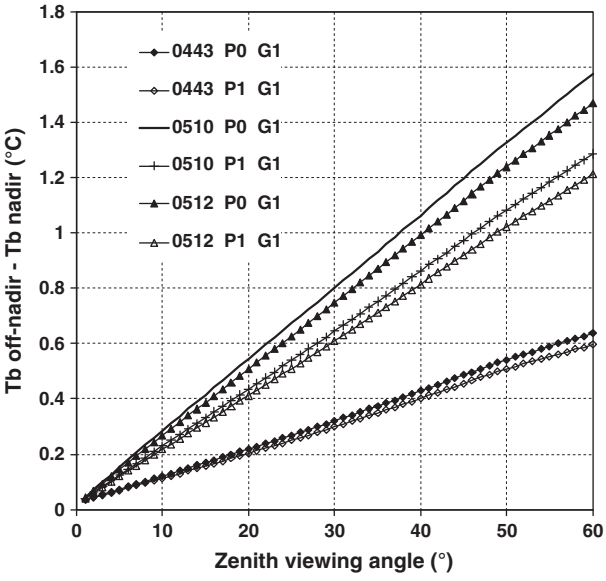

Fig. 11. Impact of uncertainties of the surface properties on the anisotropy determined with the SOLENE approach.

Practically, this, together with the good agreement observed between TEB and SOLENE simulations in our particular case study over Toulouse, allows us to use TEB simulations to generalise our results to other times in the following sections.

5. Discussion

5.1. Evolution of the anisotropy during the night

The results presented so far have been obtained in the early or middle part of the night. To assess the magnitude of the nocturnal anisotropy throughout the night, we computed the anisotropy with a 30 mn time step using surface temperatures derived from the TEB simulations. The results are given in Figs. 12 and 13 for Oct. 2–3 and Oct. 4–5 2004, the latter corresponding to the 0443 flight, and Feb. 24–25 and 25–26 2005 corresponding to flights 0510 and 0512. We observe that the anisotropy always remains less than 1.6°C (at 60° zenith view angle), and that it reaches its maximum value at different times after sunset. We also notice a rapid increase of the anisotropy at sunset and a decrease just after sunrise (indicated by arrows in the figures). The maximum night time anisotropy is approximately 1.5°C on each of Oct. 2, Feb. 24 and Feb. 25 but is lower during the night of October 4th–5th. The reason for this difference lies in the evolution of the meteorological conditions. The time evolution of air temperature, downward longwave radiation and of windspeed at the central site for the two periods are provided in Figs. 14 and 15. The windspeed is much higher on the night of Oct. 4–5 (about 6 ms^{-1} in average) compared to that on Oct 2–3 (about 1.5 ms^{-1}). By facilitating turbulent convective exchange, the effect of the wind is to reduce the thermal contrasts between the different elements of the canopy, as is demonstrated in Fig. 14: the temperatures of the roofs, walls and streets are much closer than on previous days, which results in limited anisotropy. Despite the effects

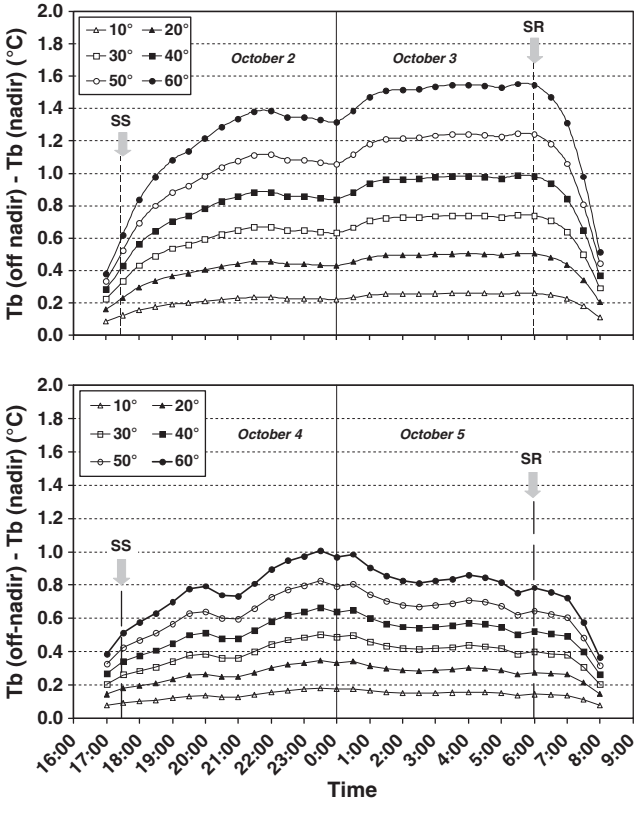

Fig. 12. Evolution of the directional anisotropy throughout the night determined using the TEB approach for 6 zenith viewing angles between 10 and 60°, for October 2–3 (up) and 4–5 (below), 2004. Sunset (SS) and sunrise (SR) times are indicated by arrows.

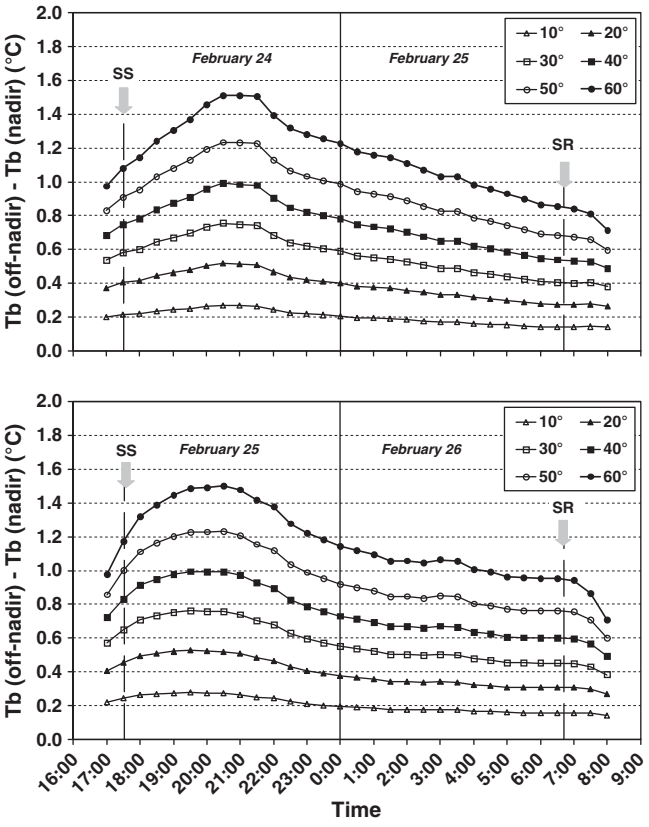

Fig. 13. Same as Fig. 12 for February 24–25 (up) and 25–25 (below), 2004.

are pretty subtle, a link between variations in wind speed and anisotropy could be suggested. During the night of October 3rd a continuous decrease in wind speed seems to contribute to a noticeable increase in the rate of roof cooling and a resultant increase in the temperature differences between roofs and other surfaces, which would in turn reinforce anisotropy. We could also suggest that the maximum anisotropy observed around midnight on October 4th is correlated with a substantial decrease in wind speed at this time (by about 1 to 1.5 ms^{-1}).

The radiative exchanges which partly govern the surface temperatures also have an impact on the anisotropy. For the night of Oct 2–3 L↓ displays some fluctuations at the beginning of the night with an average value greater by about 40 Wm^{-2} than in the second part of the night, which could be attributed to the presence of haze; this tends to limit the radiative cooling of the surface by compensating for its longwave emission, so reducing the thermal contrasts and thus the anisotropy. But in the case considered, it is difficult to separate the impact of the decrease of L↓ from midnight, from the impact of a simultaneous decrease of wind speed having a similar effect on anisotropy.

5.2. Sensitivity to thermal inertia

During daytime the sunlit facets oriented towards the Sun display higher temperatures than the shaded ones. At sunset thermal contrasts still exist within the canopy. These tend to vanish during the beginning of the night, with a time delay depending on the thermal inertia of the materials and possibly also depending on the cooling regime (intensity of convective exchanges, in particular). The question raised is: how long can these effects persist and influence the overall directional anisotropy?

To answer this question a simple modelling exercise based on SOLENE was conducted for the 0512 flight (February 25th, 2005). The

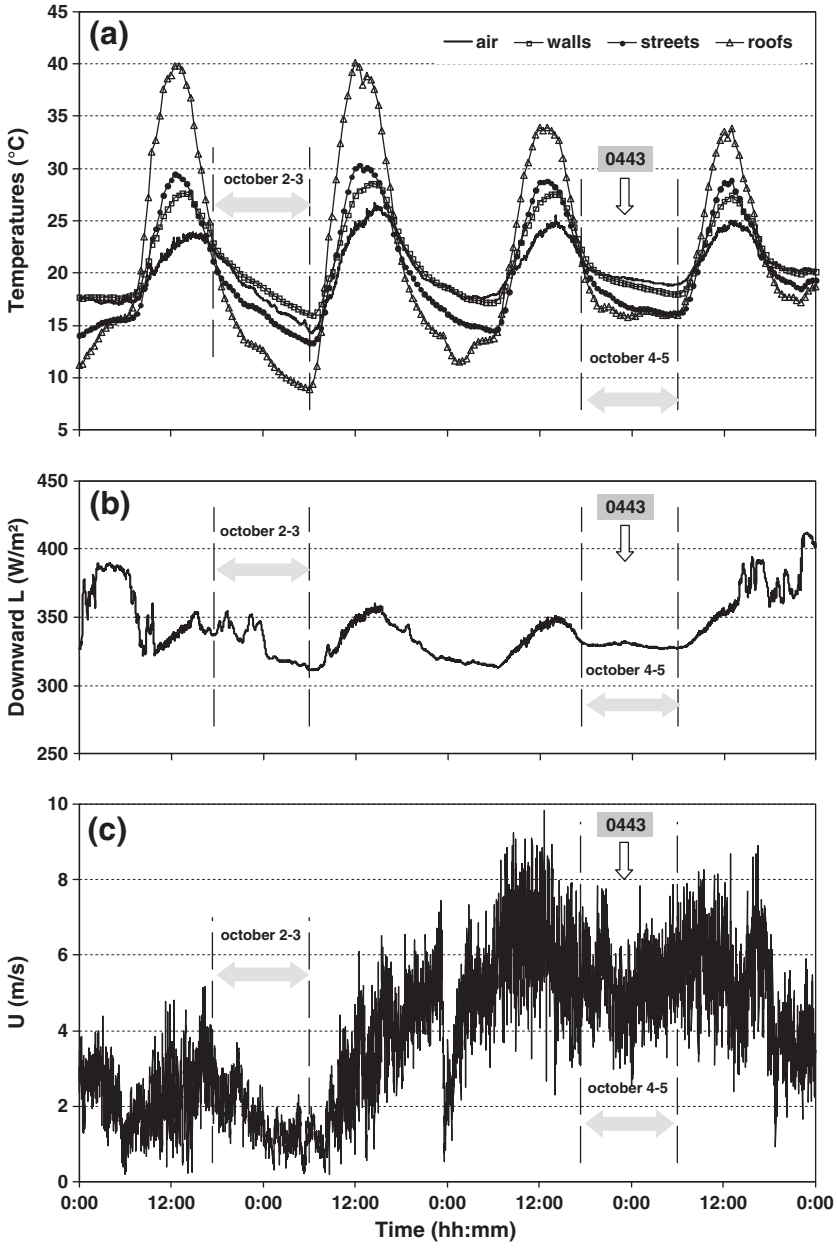

Fig. 14. TEB simulated temperatures of roofs, streets, and walls between October 2nd and 5th (a). Air temperature is also plotted. Evolution of the downward longwave radiation (b) and wind speed (c) for the same period.

simulations were performed for a set of 18 canyon streets oriented between 10 and 180° by 10° steps which represent the city structure. The resulting directional temperature for each viewing direction was then directly computed by integrating the temperatures of all the facets seen in this direction, mixing the 18 canyons all together. This approach is a simplification of that followed in Section 3.3.2, the integration now being done globally for the ensemble of 18 streets, and not by class with a weighting based on the actual 3D structure of the canopy. This method avoids the POVRAY computation step. The simulation exercise was conducted using the P0 set of parameters and the G1 canyon geometry, and temperature profiles across the canyon street were generated between 15:30 and 24:00 UTC.

Fig. 16 shows the time evolution of the temperature profile across the street oriented (167° clockwise relatively to North) perpendicularly to the Sun's azimuth (257°) at the moment of sunset. It reveals several interesting features. At 15:30 UTC the Sun elevation is just above (20.25°) the slope of the roofs. The roof facing South-West has been directly exposed to the Sun all afternoon long with a large relative incident angle: at 15:30 UTC this angle is still about 40° (with respect to the plane of the roof) whereas it is nearly 0° for the roof facing North-East. It easily explains the temperature difference of about 12°C between the two sides of roofs. At the same time only the upper part of the wall facing South-West is sunlit, and it displays a maximum temperature (about 22.5°C) even higher than that of the roof, whereas its lower part is shaded but remains warmer because of the heat stored during the afternoon. The street displays the lowest temperature because it has been shaded for a long period; it shows a slight asymmetry at 15:30, its east side being a little warmer probably associated with thermal inertia effects. The contrast in temperatures between facets progressively decreases during the late afternoon as incoming solar radiation decreases, and the roofs rapidly become the coldest surfaces after sunset (occurring at 17:32), because of radiative losses towards the sky. The thermal inertia effects can be observed until about 21:00–22:00 from which a symmetrical temperature

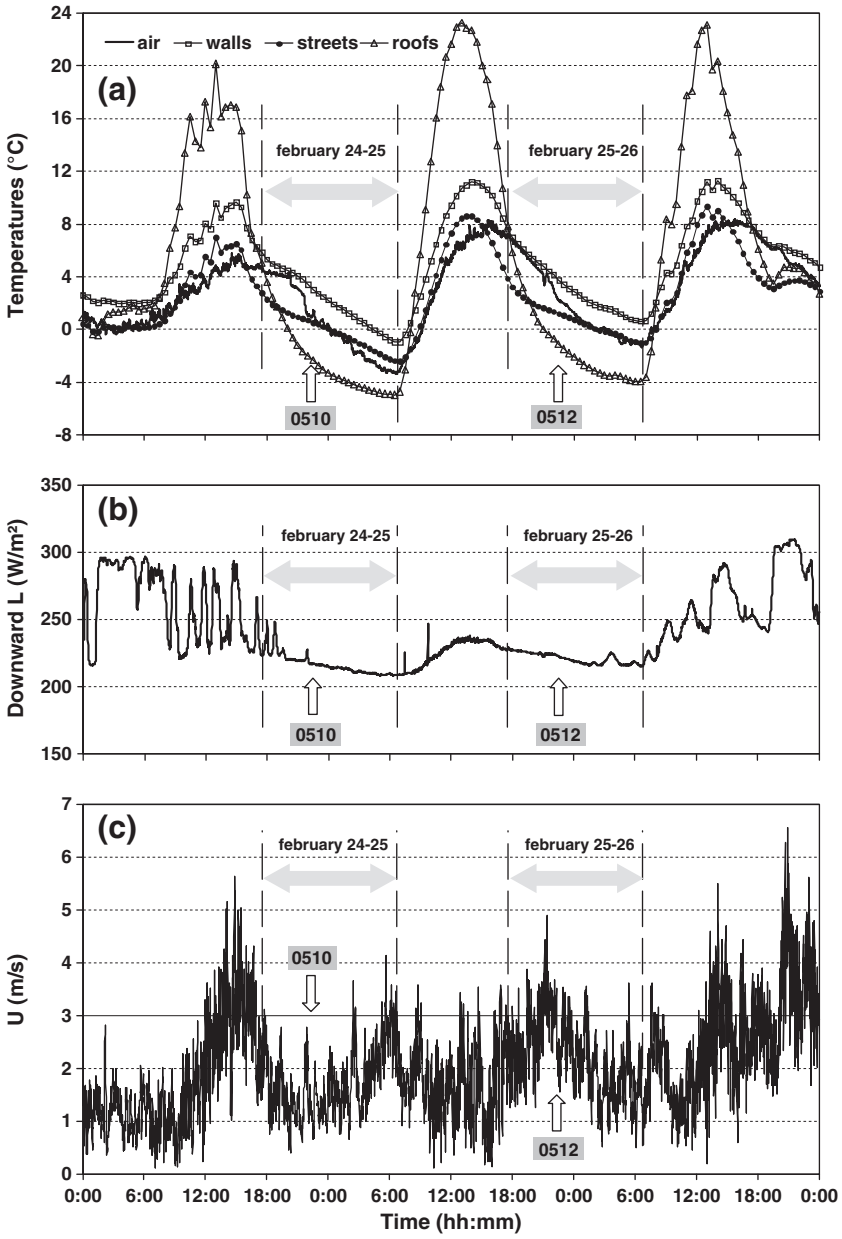

Fig. 15. Same as Fig. 14 between February 24th and 26th, 2005.

profile across the street is established. A similar behaviour is observed for the other streets, with small differences only depending on their orientations.

As a consequence, thermal inertia effects on the directional anisotropy are apparent for about 4 h after sunset in our case, with no more azimuthal dependence after about 22:00. This is illustrated in Fig. 3, right part, where the simulated polar plots of anisotropy at 15:30, 17:30, and midnight have been plotted. A detailed analysis (not illustrated here) of the complete series of the plots shows no azimuthal displacement of the region of maximum anisotropy with the Sun after 15:30. Initially unexpected, this finding is easily explained by the fact that most of the walls cease to receive direct solar radiation after this time and do not significantly contribute thereafter to the anisotropy.

Another way of illustrating the effect of the thermal behaviour of the canopy is to study the difference for a given azimuth between the 2 temperatures (or anisotropy) at opposite zenith viewing angles, one looking roughly westward, the other eastward: at the end of the afternoon, the difference should tend to decrease with time in relation with the decrease of solar radiation, and then after sunset in relation with the prevailing thermal inertia effect. To illustrate this idea, Fig. 17 presents the time evolution of the difference of anisotropy at 60° zenith viewing angles for the solar plane at sunset (corresponding to the black circles in Fig. 3, right). The differential cooling of westward and eastward facing facets with thermal inertia explains its decrease around sunset time. The insignificant difference after 21:00 or 22:00 shows the thermal history of the previous day has completely been lost by that time.

5.3. Application to satellite data

The results of this research can mainly be used by researchers that use surface temperatures in their models, for example calculating the sensible heat flux using bulk transfer approaches. For practical

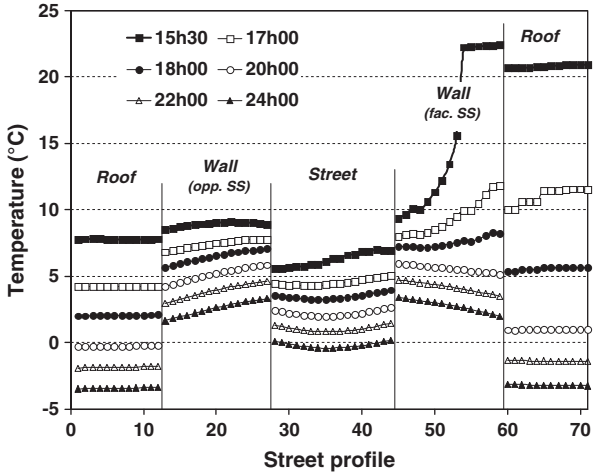

Fig. 16. Evolution of the temperatures simulated between 15:30 and 24:00 on February 25th, 2005 with SOLENE across the canyon street oriented perpendicularly to the sunset solar azimuth. The X-axis corresponds to the grid mesh index counted from the left side of the canyon (see Fig. 18b).

applications particular attention should nevertheless be paid first to the spatial resolution of the satellite data used, and second to the emissivity of urban materials.

In the methodology we developed, no notion of scale has been explicitly specified. The studied area has simply been chosen large enough (a few hundred metres) to include all the different representative features of the centre of Toulouse; moreover the flight plan adopted allowed us to integrate the contribution of the small scale local heterogeneities and structures, such as street width and orientation, differences in the size of the buildings, presence of small squares, etc. We therefore retrieved a so-called 'average' anisotropy characteristic of an old European city centre. Our results could be used directly with low resolution satellite data, such as AVHRR or MODIS, provided homogeneous 1 km² pixels can be identified in the centre of the studied cities, i.e. for rather large cities. For suburban areas displaying different canopy structures, the simulations should be repeated with corresponding 3D models to generate indicators of the TIR anisotropy. In the case of mixed 1 km² pixels, a weighting of directional temperatures over central and suburban areas will be required. The contribution of vegetation often present in suburban areas remains to be investigated. In the case of high spatial resolution TIR data, of about 50 m or so planned in HYSPIRI (http://hyspiri.jpl.nasa.gov/) or MISTIGRI (Lagouarde et al., in press) projects, the canopy cannot be considered as homogeneous at this scale; the detailed 3D canopy structure inside the pixel here needs to be taken into account, and new approaches relying on high resolution simulations of the canopy temperature such as the one illustrated by Hénon et al. (2009a,b) using SOLENE will have to be developed.

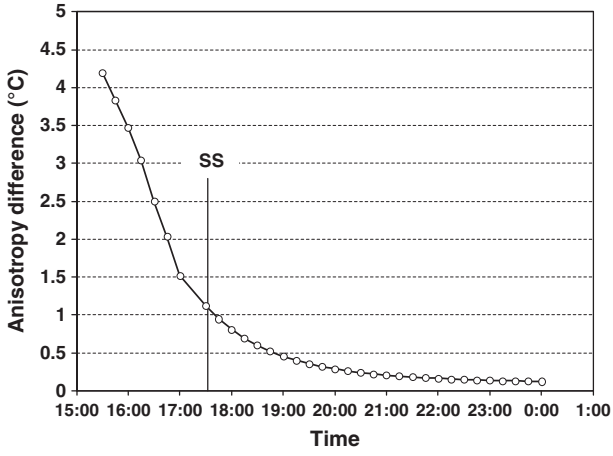

Fig. 17. Time evolution of the difference between anisotropy at opposite 60° zenith viewing angles in the sunset solar plane. SS indicates time of sunset.

The questions related to emissivity have not been addressed in our work. In fact the overall emissivity of the canopy, which is a heterogeneous and non-isothermal surface, is also subject to directionality, and should be known to retrieve the radiometric surface temperatures used in flux estimations. The problem is not trivial and the emissivity at the pixel scale depends on the viewing angles in several ways. In addition to cavity effects related to multiple reflections, the directional emissivity is governed by a weighting of the ground, wall and roof areas seen by the sensor, which all display different emissivities. Moreover the urban surfaces include artificial materials (concrete, glass, metal, etc.) that have significant contrasts in their spectral properties. The sensitivity to these combined effects results in an 'ensemble directional emissivity' (Norman and Becker, 1995). These effects could be studied using available modelling tools such as TITAN (Fontanilles et al., 2008) to analyse and evaluate the main spectral radiative fluxes contributing to the total spectral signal received by a sensor observing a complex surface in the 3 to 14 μm spectral domain. Multi spectral TIR instruments including bands in the 8–10 μm domain in which spectral emissivities display the largest variability should help to evaluate their impact on directional anisotropy of measured surface temperatures.

6. Conclusion

This paper presents an original study of nighttime TIR directional anisotropy over an urban area. The first part describes the experimental results obtained during the middle of 3 fall and winter nights (October 5th, 2004, and February 24 and 25, 2005) over the old core of Toulouse, using the methodology of Lagouarde et al. (2010, 2004). The results reveal that the off nadir — nadir brightness temperature differences at ground level (i.e. after correction of aircraft data from atmospheric effects) remains lower than 2°C over the range of zenith viewing angles (up to 60°) studied, with no azimuthal dependence observed.

In a second step we proposed a modelling approach based on the combination of a 3D model of the urban canopy providing the ratios of the different surface types seen in a given direction with an urban canopy energy balance model providing the temperature of the facets. Two canopy models have been tested. The TEB model (developed at Météo France) simulates a simple canyon street geometry with 3 classes of surface (facet) types only (street, walls, and flat roofs). TEB does not include sub-facet temperature variability, limiting the assessment of temperature variabilities of a particular facet type and the discrimination between sunlit/shaded zones during daytime. All street orientations are assumed to be present, and this is taken into account by averaging the angular-dependent input variables for simulations. The SOLENE model (developed at CERMA Nantes) can generate realistic surface temperature fields over actual complex geometries of canopies discretized as a number of independent facets for which computations of fluxes and temperatures are repeated (Hénon et al., 2009a,b). However, because of computing time limitations, SOLENE was used in a simplified manner; simulations were first performed for an ensemble of equivalent canyon streets in all directions, and they were integrated for deriving directional temperatures by class (streets, walls, roofs); these were finally aggregated according to their class ratios determined from images generated using the 3D model and POV-Ray software. After having tested the possible impact of uncertainties on the geometry of the equivalent canyon street considered and on the value of some of the input surface properties, the simulations revealed quite robust results

with both TEB and SOLENE approaches that led to a good agreement with the airborne measurements of anisotropy.

An extension of the results to the whole night was proposed using the TEB approach, and an evaluation of the effect of the thermal inertia after sunset was also done using the SOLENE approach. It shows that the anisotropy remains lower than 2°C for the entire night for the periods we studied. An analysis of micrometeorological conditions illustrating the influence of the wind and incoming longwave radiation was also presented. Moreover we showed that 3 to 4 h after sunset the influence of the differences in wall temperatures resulting from the Sun heating during the previous day has completely disappeared, and that radiative exchanges prevail from this moment. This is true for the winter and fall conditions we studied, because Sun elevation is low. Tests should be done with the proposed model for performing simulations exercises in summertime conditions for which we may not fully lose the azimuthal dependence of temperature over the night in-canyon temperature measurements: for instance canyon temperature measurements performed in the BUBBLE project (Rotach et al., 2005) revealed that the base of south-facing walls and the canyon floor surface near them remained warmer throughout the entire night in July.

Additional studies are necessary to evaluate the anisotropy for other canopy structures (different aspect ratios, steeper roofs…) and climatic conditions. The SOLENE approach here offers a very practical tool, more adapted than TEB, for this purpose. Moreover it could easily be adapted to the case of cities displaying important differences of structural features, such as a few prevailing street directions or types (for instance rectangular pattern of Northern American towns, presence of large 'boulevards'), or variations between districts (average height of buildings for instance).

However we must recall that for simplicity, the simulation strategy described in this paper is based on an aggregation of temperatures performed at the 'class' scale. In the future, expected progress in both computing performance and models able to simulate high resolution canopy temperatures will allow a direct and more realistic aggregation at the facet scale. These advances will facilitate the study of directional temperatures over heterogeneous areas. Important work nevertheless still remains to be done on the determination of input thermo-radiative properties, on the introduction of vegetation within built areas, etc., and finally on the validation of the models involved themselves.

Athough the amplitude of nightttime directional anisotropy is only 2°C and may appear small, it may be crucial to correct remotely sensed data for anisotropy for some practical applications. As a matter of fact surface *minus* air temperature gradients being generally small during nighttime, partly because of the roughness of urban canopies, such an uncertainty may have a strong impact on the estimation of the surface fluxes – sensible heat, storage and anthropogenic fluxes – which are particularly important for applications such as evaluating the energy consumption needs in winter conditions or frost forecasting for instance.

Acknowledgements

This work received support from the PNTS (Programme National de Télédétection Spatiale) and INSU/CNRS (Institut National des Sciences de l'Univers). The CAPITOUL project (http://medias.cnrs.fr/capitoul/) was placed under the responsibility of Météo France. The second author benefitted of a doctoral grant from CNRS and the Region Pays de la Loire and a post-doctoral grant from the same Region within the IRSTV project MEIGEVille. The authors thank the SAFIRE group for their contribution to the airborne measurements. They gratefully acknowledge all the people involved in ground measurements and radiosoundings during the flights. They also thank the 'Mairie de Toulouse' for providing the 3D data base of the city.

Appendix A. Generating the directional brightness temperatures by class from SOLENE simulations

The SOLENE simulations provide profiles of brightness temperatures across the street, perpendicular to it (ABEFIJ, in Fig. 18). The grid meshs are referred to by 2 indices, *i* counted from A corresponds to the grid mesh rank in the profile while *k* indicates the street direction. For each grid mesh, the simulated temperature is denoted as $T_{i,k}$. A normal unit vector $N_{i,k}$ is computed for each grid mesh. The azimuth of the street is 10(*k*-1) counted clockwise from North.

For a given viewing direction, the temperatures simulated over the ensemble of the 18 street directions are weighted by the surface area of the corresponding facets and integrated to compute a directional brightness temperature. This weighting is performed for each of the 3 surface types (roofs, ground, walls).

Integration of the temperature of roofs for a viewing direction

The average temperature of roofs $T_r(\theta_v,\varphi_v)$ for the (θ_v,φ_v) viewing direction results from 2 integrations, the first one along the roof profile of the canyon street and the second one for the ensemble of canyon street directions. The computation is based on a Stefan-Boltzmann law aggregation scheme:

$$[T_r(\theta_v,\varphi_v)]^4 = \frac{\sum_k \sum_i s_{i,k}\left[T_{i,k}\right]^4 \vec{N}_{i,k}.\vec{V}}{\sum_k \sum_i s_{i,k}\ \vec{N}_{i,k}.\vec{V}} \text{ with } \begin{matrix} i \in [AB] \cup [IJ] \\ k \in [1,18] \end{matrix} \quad \text{(A1)}$$

where $s_{i,k}$ is the surface of the grid mesh, 1m² in our case, and $\vec{V}$ the viewing direction unit vector directed towards the outside of the canyon street.

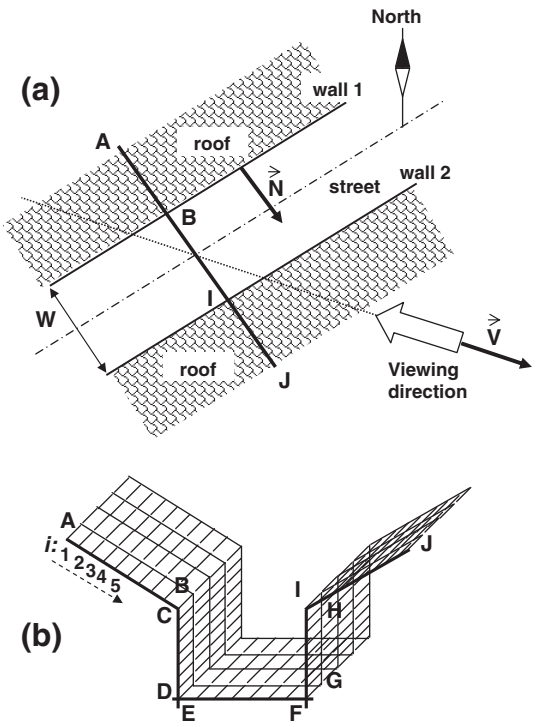

Fig. 18. Schematic views of the canyon street from above (a) and in profile (b). AB and IJ segments correspond to roofs both sides of the canyon, CD and GH to opposite walls and EF to the street.

Integration of the temperature of streets and walls for a viewing direction

The geometry of the canyon streets means that some portions of street and wall facets remain hidden to direct observation. These are easily identified as they correspond to negative values of the scalar product $\overrightarrow{N_{i,k}}.\overrightarrow{V}$. In such cases the scalar product is forced to 0. Occultation of some facets may also result from the presence of obstacles between them and the observer: the walls may be seen only partially and the street possibly not at all, depending on the height of neighbouring walls, the length of the street section seen in the azimuthal viewing direction and the zenithal viewing angle. Simple geometrical computations allow us to attribute to any pixel of the canyon street (walls and ground) an index $\alpha_{i,k}$ for which the value is 1 (0) when the pixel is seen (occulted).

For sunlit walls, the averaged brightness temperature $T_w(\theta_v,\varphi_v)$ is determined as:

$$[T_w(\theta_v,\varphi_v)]^{1/4} = \frac{\sum_k \sum_i s_{i,k}\,\alpha_{i,k}\left[T_{i,k}\right]^4 \overrightarrow{N_{i,k}}.\overrightarrow{V}}{\sum_k \sum_i s_{i,k}\,\alpha_{i,k}\,\overrightarrow{N_{i,k}}.\overrightarrow{V}} \text{ with } \begin{array}{l} i \in [CD]\cup[FI] \\ k \in [1,18] \end{array} \quad \text{(A2)}$$

The same equations hold with $i\in[EF]$ to compute the street temperatures $T_{str}(\theta_v,\varphi_v)$.

The $T_w(\theta_v,\varphi_v)$, $T_{str}(\theta_v,\varphi_v)$ and $T_r(\theta_v,\varphi_v)$ derived brightness temperatures correspond to the $T_{b,i}$ temperatures in Eq. (2).

References

Becker, F., & Li, S. L. (1995). Surface temperature and emissivity at various scales: Definition, measurement and related problems. *Remote Sensing Reviews*, *12*, 225–253.

Carlson, T. N., & Arthur, S. T. (2000). The impact of land use-land cover changes due to urbanization on surface microclimate and hydrology: A satellite perspective. *Global and Planetary Change*, *25*, 49–65.

Cros, B., Durand, P., Cachier, H., Drobinski, P., Fréjafon, E., Kottmeïer, C., et al. (2004). The ESCOMPTE program: An overview. *Atmospheric Research*, *69*(3–4), 241–279.

Fontanilles, G., Briottet, X., Fabre, S., & Trémas, T. (2008). Thermal infrared radiance simulation with aggregation modelling (TITAN): An infrared radiative transfer model for heterogeneous 3-D surface — application over urban areas. *Applied Optics*, *47*(31), 5799–5810.

Henon A. (2008). Températures mesurées, modélisées et observées par télédétection infrarouge dans la canopée urbaine: modélisation aéro-thermoradiative des flux de chaleur urbains. *PhD Thesis*, École Centrale de Nantes et Université de Nantes. 251 pp.

Hénon, A., Lagouarde, J. P., Mestayer, P., & Groleau, D. (2009). High resolution surface temperature and urban thermal anisotropy simulations: Validation against airborne remote sensing TIR data over Toulouse city (France). *8th AMS Symp. on Urban Environment, Phoenix AZ, poster session*.

Hénon, A., Mestayer, P. G., Groleau, D., & Voogt, J. (2011). High resolution thermo-radiative modeling of an urban fragment in Marseille city center during the UBL-ESCOMPTE campaign. *Building and Environment*, *46*, 1747–1764.

Hénon, A., Mestayer, P., Lagouarde, J. P., & Lee, J. H. (2009). Anisotropy of thermal infrared remote sensing over urban areas: Assessment from airborne data and modelling approach. *EMS Annual Meeting Abstracts, 9th EMS / 9th ECAM, Vol. 6*, EMS2009-110-2. poster.

Huband, N. D. S., & Monteith, J. L. (1986). Radiative surface temperature and energy balance of a wheat canopy. *Boundary-Layer Meteorology*, *36*, 1–17.

Kneisys, F. X., Shettle, E. P., Abreu, L. W., Chetwynd, J. H., & Anderson, G. P. (1988). *User's guide to LOWTRAN 7*. Report A377602. Air force geophysics lab., Hanscom AFB, MA, USAhttp://www.stormingmedia.us/37/3776/A377602.html.

Lagouarde, J. P., Ballans, H., Moreau, P., Guyon, D., & Coraboeuf, D. (2000). Experimental study of brightness surface temperature angular variations of maritime pine. *Remote Sensing of Environment*, *72*, 17–34.

Lagouarde, J. P., Hénon, A., Kurz, B., Moreau, P., Irvine, M., Voogt, J., et al. (2010). Modelling daytime thermal infrared directional anisotropy over Toulouse city centre. *Remote Sensing of Environment*, *114*, 87–105.

Lagouarde, J. P., & Irvine, M. (2008). Directional anisotropy in thermal infrared measurements over Toulouse city centre during the CAPITOUL measurement campaigns: First results. *Meteorology and Atmospheric Physics*, *102*, 173–185, doi: 10.1007/s00703-008-0325-4 special issue CAPITOUL.

Lagouarde, J. P., Moreau, P., Irvine, M., Bonnefond, J. M., Voogt, J. A., & Solliec, F. (2004). Airborne experimental measurements of the angular variations in surface temperature over urban areas: Case study of Marseille (France). *Remote Sensing of Environment*, *93*, 443–462.

Lagouarde J.P., Bach M., Sobrino J.A., Boulet G., Briottet X., Cherchali S., Coudert B., Dadou I., Dedieu G., Gamet P., Hagolle O., Jacob F., Nerry F., Olioso A., Ottlé C., Roujean J.L., & Fargant G. (in press). The MISTIGRI Thermal Infrared project: scientific objectives and mission specifications. *International. Journal of Remote Sensing.*

Lemonsu, A., Bélair, S., Mailhot, J., & Leroyer, S. (2010). Evaluation of the town energy balance model in cold and snowy conditions during the Montreal urban snow experiment 2005. *Journal of Applied Meteorology and Climatology*, *49*, 346–362, doi: 10.1175/2009JAMC2131.1.

Lemonsu, A., Grimmond, C. S. B., & Masson, V. (2004). Modeling the surface energy balance of the core of an old Mediterranean city: Marseille. *Journal of Applied Meteorology*, *43*, 312–327.

Leroyer, S., Mailhot, J., Bélair, S., Lemonsu, A., & Strachan, I. B. (2010). Modeling the surface energy budget during the thawing period of the 2006 Montreal urban snow experiment. *Journal of Applied Meteorology and Climatology*, *49*, 68–84, doi: 10.1175/2009JAMC2153.1.

Li, X., Strahler, A. H., & Friedl, M. A. (1999). A conceptual model for effective directional emissivity from nonisothermal surfaces. *IEEE Transactions on Geoscience and Remote Sensing*, *37*(5), 2508–2517.

Masson, V. (2000). A physically-based scheme for the urban energy budget in meteorological models. *Boundary-Layer Meteorology*, *94*, 357–397.

Masson, V., Gomes, L., Pigeon, G., Liousse, K., Pont, V., Lagouarde, J. -P., et al. (2008). The canopy and aerosol particles interactions in Toulouse urban layer (CAPITOUL) experiment. *Meteorology and Atmospheric Physics*, *102*, 135-15.

Masson, V., Grimmond, C. S. B., & Oke, T. R. (2002). Evaluation of the town energy balance (TEB) scheme with direct measurements from dry districts in two cities. *Journal of Applied Meteorology*, *41*, 1011–1026.

Mestayer, P. G., Durand, P., Augustin, P., Bastin, S., Bonnefond, J. M., Bénech, B., et al. (2005). The urban boundary-layer field campaign in Marseille (UBL/CLU-ESCOMPTE): Set-up and first results. *Boundary-Layer Meteorology*, *114*, 315–365.

Norman, J. M., & Becker, F. (1995). Terminology in thermal infrared remote sensing of natural surfaces. *Agricultural and Forest Meteorology*, *77*, 153–166.

Pigeon, G., Legain, D., Durand, P., & Masson, V. (2007). Anthropogenic heat releases in an old European agglomeration (Toulouse, France). *International Journal of Climatology*, *27*, 1969–1981.

Pigeon, G., Moscicki, M. A., Voogt, J. A., & Masson, V. (2008). Simulation of fall and winter surface energy balance over a dense urban area using the TEB scheme. *Meteorology and Atmospheric Physics*, *102*, 159–171.

Rotach, M. W., Vogt, R., Bernhofer, C., Batchvarova, E., Christen, A., Clappier, A., et al. (2005). BUBBLE — An urban boundary layer meteorology project. *Theoretical and Applied Climatology*, *81*, 231–261.

Roth, M., Oke, T. R., & Emery, W. J. (1989). Satellite-derived urban heat islands from three coastal cities and the utilization of such data in urban climatology. *International Journal of Remote Sensing*, *10*(11), 1699–1720.

Soux, A., Voogt, J. A., & Oke, T. (2004). A model to calculate what a remote sensor 'sees' of an urban surface. *Boundary-Layer Meteorology*, *111*, 109–132.

Voogt, J. A. (2008). Assessment of an urban sensor view model for thermal anisotropy. *Remote Sensing of Environment*, *112*, 482–495.

Voogt, J. A., & Oke, T. R. (2003). Thermal remote sensing of urban climates. *Remote Sensing of Environment*, *86*, 370–384.